Austenitic stainless steels and high strength copper alloys for fusion components

A.F. Rowcliffe [a,*], S.J. Zinkle [a], J.F. Stubbins [b], D.J. Edwards [c], D.J. Alexander [a]

[a] *Oak Ridge National Laboratory, P.O. Box 2008, Bldg. 5500, Oak Ridge, TN 37831-6376, USA*
[b] *University of Illinois, Department of Nuclear Engineering, 103 S. Goodwin, Urbana, IL 61801, USA*
[c] *Pacific Northwest National Laboratory, P.O. Box 999, Richland, WA 99352, USA*

Abstract

An austenitic stainless steel (316LN), an oxide-dispersion-strengthened copper alloy (GlidCop Al25), and a precipitation-hardened copper alloy (Cu–Cr–Zr) are the primary structural materials for the ITER first wall/blanket and divertor systems. While there is a long experience of operating 316LN stainless steel in nuclear environments, there is no prior experience with the copper alloys in neutron environments. The ITER first wall (FW) consists of a stainless steel shield with a copper alloy heat sink bonded by hot isostatic pressing (HIP). The introduction of bi-layer structural material represents a new materials engineering challenge; the behavior of the bi-layer is determined by the properties of the individual components and by the nature of the bond interface. The development of the radiation damage microstructure in both classes of materials is summarized and the effects of radiation on deformation and fracture behavior are considered. The initial data on the mechanical testing of bi-layers indicate that the effectiveness of GlidCop Al25 as a FW heat sink material is compromised by its strongly anisotropic fracture toughness and poor resistance to crack growth in a direction parallel to the bi-layer interface. © 1998 Elsevier Science B.V. All rights reserved.

1. Introduction

Austenitic stainless steels and high strength copper alloys are the primary structural materials for the in-vessel components of ITER. The ITER first wall/blanket system consists of 739 modules, each weighing 4.3 tons, attached to a supporting back plate. The blanket system also includes limiter and baffle modules, and the entire system is cooled with water at 140°C. The primary structural material for the blanket system is an austenitic stainless steel, designated 316LN-IG. Selection of this material is backed by some 20–30 years of operating experience in the nuclear environments of light water and fast breeder reactors; the rationale for this selection has been presented by Tavassoli [1].

The main modules must dissipate a heat flux of ~0.5 MW/m^2; the heat fluxes to the baffle and limiter modules are ~3 and ~8 MW/m^2, respectively [2]. To facilitate the uniform dissipation of these heat fluxes, a copper alloy heat sink is bonded to the primary wall using the process of hot isostatic pressing (HIP). The current choice of material for the FW heat sink is GlidCop Al25, an oxide-dispersion-strengthened alloy fabricated by hot extrusion of powders, followed by cold working [3]. In contrast to the 316LN-IG, there is no prior operating experience for GlidCop in a nuclear environment or indeed in any structural application at temperatures in the range 100–350°C.

The divertor system consists of 60 cassettes. Each cassette is a complex, multi-component system measuring approximately 2 m high, 5 m long, and 0.75 m wide. The main body of the cassette is fabricated from 316LN-IG by casting, followed by a HIP consolidation. Heat fluxes in some regions of the divertor may be as high as 15 MW/m^2, so that a heat sink material with high conductivity and high thermal stress resistance is critically important. The current primary choice for the vertical target, liner, and dome is a Cu–Cr–Zr alloy in a solution treated and aged condition. This material was used extensively in the construction of JET, but there is no prior operating experience in a neutron environment.

*Corresponding author. Tel.: +1 423 574 5057; fax: +423 574 0641; e-mail: af8@ornl.gov.

Although the neutron doses in the Basic Performance Phase (BPP) are relatively low (0.5–3.0 dpa), the accumulation of radiation damage leads to very significant changes in the deformation behavior and fracture behavior of both classes of material. In the following, the essential features of the radiation damage structure in stainless steels and copper alloys are compared, and the relationship between the damage structure and the changes in deformation mode and mechanical behavior are discussed. The differences in response to radiation damage will strongly influence the mechanical performance of the thick-section bi-layer being considered for the ITER first wall (FW).

2. Radiation damage in austenitic stainless steels

The development of the radiation damage and precipitate structure as a function of neutron dose and temperature has been reviewed by Maziasz [4] and by Zinkle et al. [5]. The damage structure in stainless steels is complex; at least six different planar and three-dimensional interstitial and vacancy defects have been analyzed and at least eight radiation-induced, or radiation-modified phases have been identified [6]. The ITER components will operate in the low temperature damage regime, which extends from the onset of vacancy motion (annealing Stage III) up to temperatures where vacancy clusters created in the displacement cascade become thermally unstable (annealing Stage V). This regime (~50–300°C) is below the usual temperature range for significant void swelling, and phase transformations driven by radiation-induced segregation are unlikely. The temperature dependence of the saturation densities of the various defects is shown in Fig. 1 [5]. Below ~200°C, radiation damage is manifested in the form of small defect clusters, 1–2 nm in diameter (black spots). Cluster densities exceed 10^{23} m^{-3} at small fractions of a dpa. It has been shown that in an Fe–Cr–Ni alloy, the defect structure at 100–200°C is dominated by stacking fault tetrahedra (SFT), with ~20% of the defects being small interstitial loops; the fraction of SFTs decreases
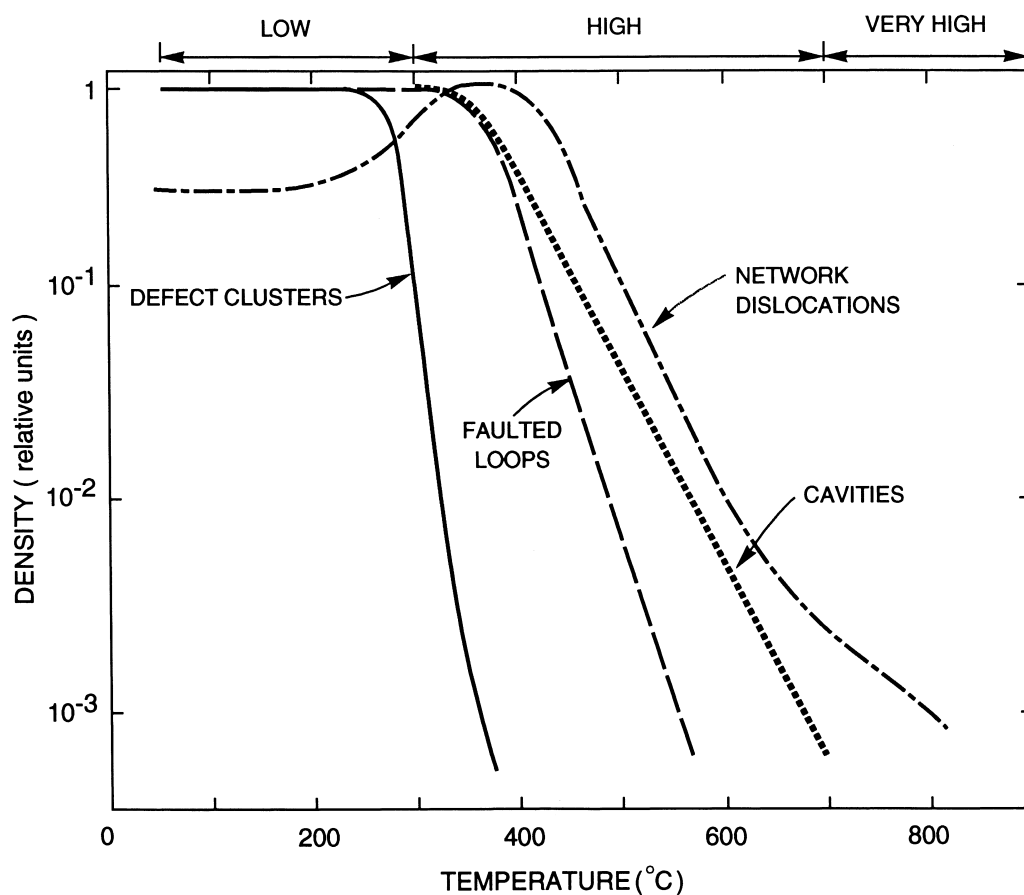
Fig. 1. Relative saturated densities of the various components of the radiation damage in austenitic stainless steels as a function of irradiation temperature.
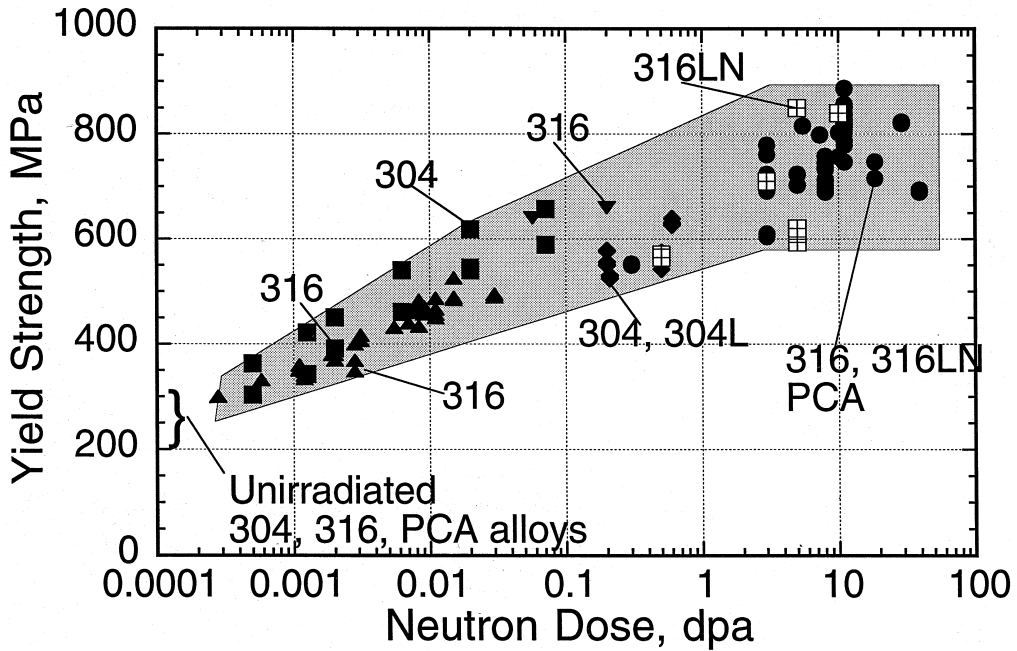
Fig. 2. Yield strength as a function of neutron dose for several annealed austenitic stainless steels (Types 316, 304, Ti-stabilized) irradiated in various neutron spectra and tested at the irradiation temperature [9].

with increasing irradiation temperature [7]. Above 250°C, the number density of defect clusters falls rapidly and faulted Frank $\langle 1\,1\,1 \rangle$ loops, 10–20 nm diameter, become the dominant feature. Small cavities, stabilized by oxygen or helium, are detectable at ~300°C and cavity number densities of the order 10^{23} m^{-3} have been reported at 350°C. At higher temperatures the number density of small cavities decreases strongly as conversion to bias-driven voids occurs; the number density of faulted loops also decreases rapidly.

In the regime of primary interest for ITER components (100–250°C), the damage structure (clusters, SFTs, and Frank loops) gives rise to a rapid increase in yield stress with increasing neutron dose, and an approach to saturation at ~1 dpa (Fig. 2). At much higher doses beyond the ITER range, there are indications that, as the microstructure coarsens, yield stress begins to decrease again (see Ref. [8] for a review). The temperature dependence of the "saturated" yield stress is shown in Fig. 3, which includes data for several alloys [9]. The irradiated YS is fairly independent of temperature up to ~200°C, and then increases to a maximum in the vicinity of 300–330°C. This maximum in hardening correlates with maxima in the number density of faulted Frank loops and small cavities.

The large increases in YS are accompanied by temperature-dependent changes in deformation mode. While the radiation-induced increases in YS do not degrade mechanical performance, the changes in defor-

mation mode can have a deleterious impact on the load bearing capability of the stainless steel structure. Engineering stress–strain curves for a 316 stainless steel irradiated to ~7 dpa are shown in Fig. 4. At 60°C, following an initial yield drop, the material work hardens at a much lower rate than in the unirradiated condition. However, the uniform strain, measured to the point of plastic instability, remains high (~30%). This implies that when the microstructure is dominated by small interstitial clusters and SFTs (1–2 nm in dia), deformation remains fairly homogeneous. However, the
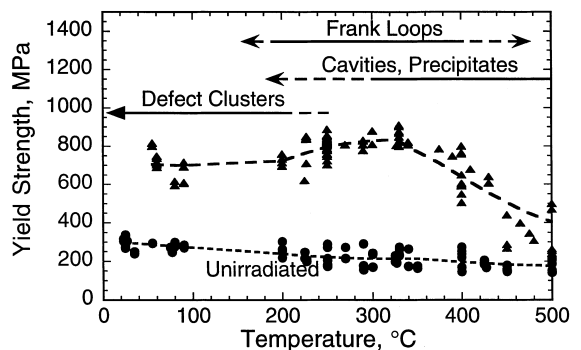
Fig. 3. Yield strength as a function of temperature for several annealed stainless steels (Types 316, Ti-stabilized) irradiated in various neutron spectra and tested at the irradiation temperature [9].
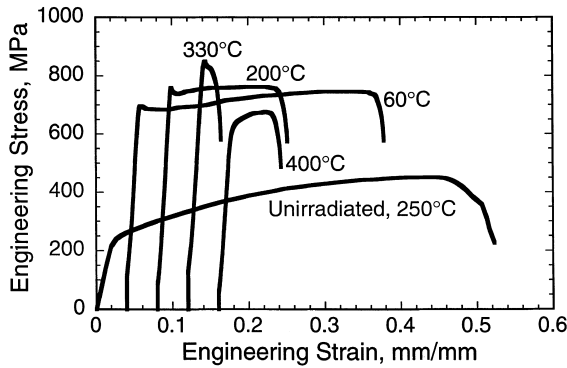
Fig. 4. Engineering stress–strain curves for SA 316 stainless steel irradiated to ∼7 dpa. The irradiation and test temperature are the same.

situation changes progressively with increasing irradiation and test temperature. At 200°C, the upper yield point and UTS are approximately the same and there is essentially no strain hardening; plastic instability does not occur, however, until a substantial level of uniform strain (∼13%) has taken place. At 330°C, the microstructure is dominated by faulted Frank loops and by small cavities at densities of ∼10^{23}/m^{-3}, and strain softening occurs immediately after yielding. This progressive increase in flow localization with increasing temperature is presumably related to an increasing shearable defect density and the formation of more widely spaced defect-free bands where dislocation channeling occurs.

The severe loss of strain hardening capacity and reduction in uniform strain are important because they impact the distribution of plastic strain at discontinuities in structural components [10]. Operation within the temperature-dose regime where intense flow localization occurs requires modification to engineering design rules to protect the structure against low ductility failure [11]. In Fig. 5, the available data on uniform strain for a range of austenitic stainless steels is plotted in the form of a dose–temperature map that defines ductile ($\varepsilon_u > 5\%$), semi-brittle ($1\% < \varepsilon_u < 5\%$) and brittle ($\varepsilon_u < 1\%$) regimes. It can be seen that for the proposed operating range of the ITER BPP (2–3 dpa), the 316LN-IG will maintain ductile behavior. However, further operation to 10 dpa and beyond may place components in a regime where the effects of flow localization must be accounted for.

The fracture toughness and tearing modulus values for austenitic stainless steels in the unirradiated condition are very high [12]. Although these parameters decrease with increasing dose in the 60–300°C temperature regime, K_J values remain above 200 MPa $\sqrt{m}$ for irradiations to ∼3 dpa [13]. A correlation between change in K_J and changes in tensile parameters has been suggested by Lucas [14]

$$K_{IC}^I / K_{IC}^U \sim \sqrt{(\varepsilon_u^i / \varepsilon_u^u)(\sigma_o^i / \sigma_o^u)},$$
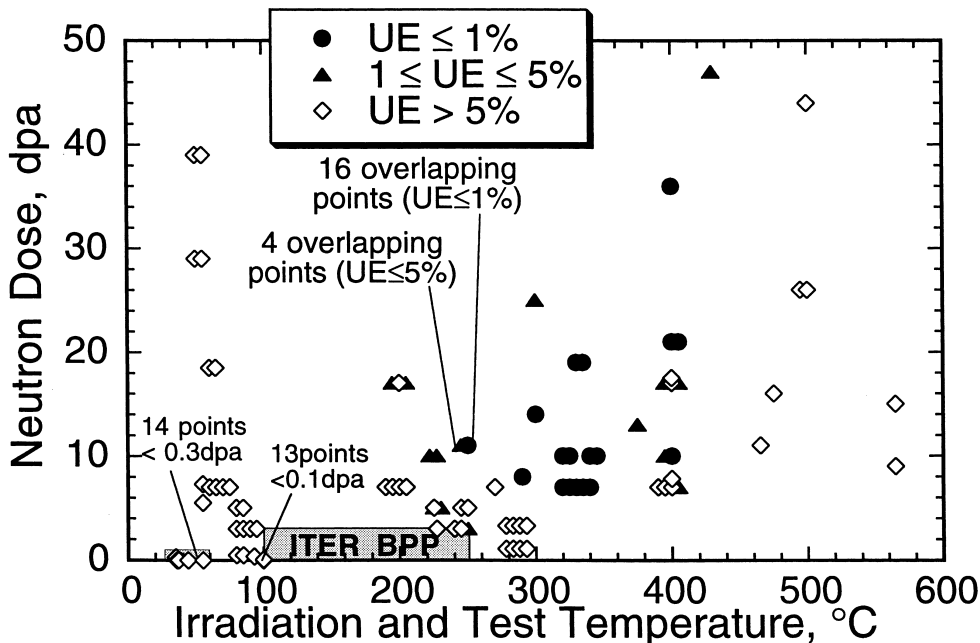
Fig. 5. Neutron dose irradiation temperature map for uniform strain (E_u) showing the regime where E_u falls below 1% [9].

where σ_o is the flow stress. The superscripts i, u indicate irradiated and unirradiated properties. Further experiments in the High Flux Reactor are being conducted under the EU ITER project, which will allow validation of this correlation at neutron doses and temperatures where severe flow localization occurs. However, it is clear that for the BPP (up to ~3 dpa) the austenitic stainless steel structure will retain a very high level of resistance to crack propagation.

3. Radiation damage in copper alloys

Microstructural evolution in neutron-irradiated copper and copper alloys has been widely studied [15–17]. The damage structure is not as complex as in stainless steels and for the temperatures relevant to the ITER FW (160–185°C for the burn cycle), the microstructure is dominated by small defect clusters of the order 2 nm in diameter. The cluster density reaches a saturation level at $\sim 10^{24}$ m^{-3} for damage levels of ~0.1 dpa for irradiation temperatures <130°C. The majority of the defect population in this regime are SFTs and the density of large loops and network dislocations is very low. For temperatures above Stage V annealing (~150°C), the defect cluster density falls sharply due to thermal evaporation from the vacancy clusters formed in the cascades. The void-swelling regime extends approximately from 180°C to 500°C, and in general the FW heat sink will operate at the low end of this range and swelling is not perceived as a significant problem. The number of small defect clusters is not strongly affected by the presence of solute concentrations of several percent, however, the fraction of defects in the form of SFT is significantly reduced [18].

Thus, for irradiation temperatures $\leqslant 200$°C, the damage microstructure in the austenitic stainless steels and copper alloys is qualitatively similar, although in stainless steel, the fraction of SFTs is lower and the mean size of defects is smaller. Fig. 6 compares the
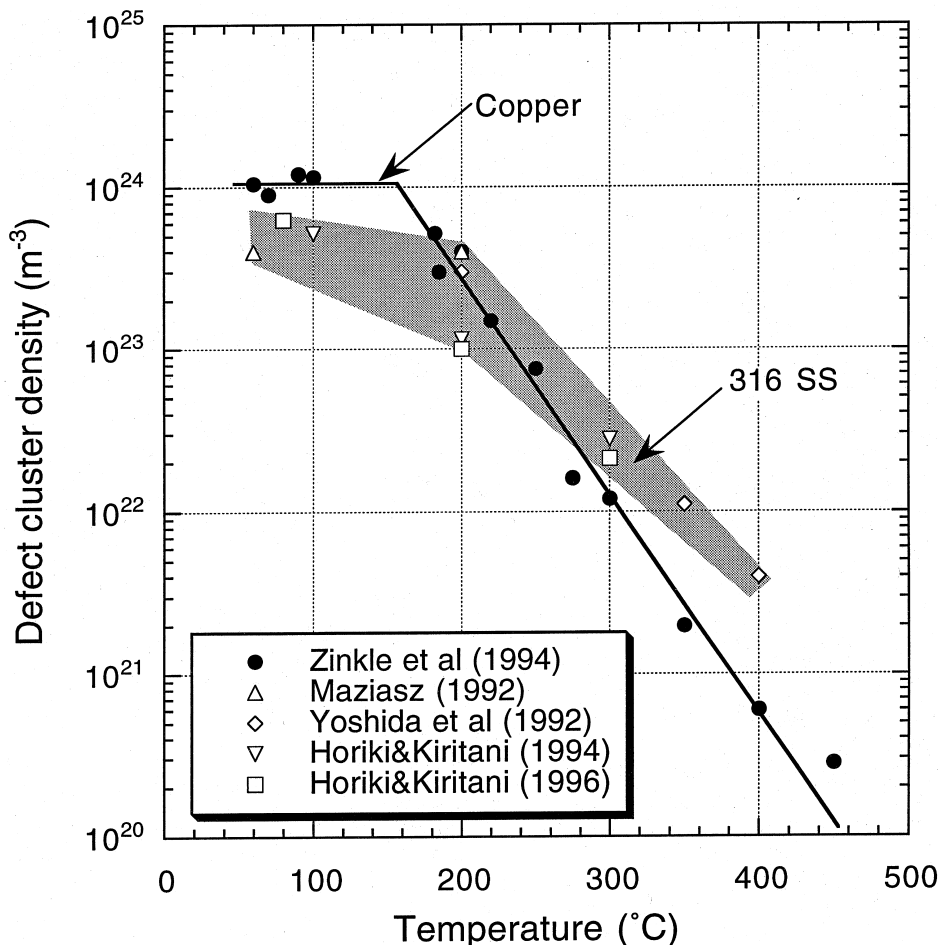
Fig. 6. The temperature dependence of saturated defect cluster densities in pure Cu and in 316 stainless steel irradiated to ~0.1 dpa.

temperature dependence of the defect densities in the two materials for doses in the range 0.1–5 dpa. In spite of the similarity in microstructure, the deformation behavior of the two materials irradiated in this regime is quite different.

Irradiation of pure copper, the precipitation hardened (PH) and oxide-dispersion-strengthened (ODS) alloys at temperatures below ∼200°C (i.e. where the saturation defect cluster-density is >10^{23} m^{-3}) results in radiation hardening accompanied by a very rapid decline in the ability of the materials to strain harden or to sustain significance levels of uniform strain before the onset of plastic instability. This occurs for irradiation at ⩽ 200°C to doses in the range 0.01–0.1 dpa, as illustrated in Fig. 7. At higher irradiation temperatures, the magnitude of the radiation hardening decreases and uniform strains begin to increase as the materials enter a transition regime at ∼300°C above which radiation softening occurs. The GlidCop alloys are markedly more resistant to radiation-induced softening than Cu–Cr–Zr (Fig. 8).

The dose dependence of radiation hardening in the copper alloys and in Type 316 stainless steels is compared in Fig. 9 for irradiation in the range 25–150°C. There is a considerable region of overlap, although copper alloys approach saturation at a much faster rate than the stainless steels, and yield strengths are significantly greater than the stainless steels for doses up to ∼0.1 dpa. Beyond ∼0.1 dpa, the yield strengths of the steels tend to exceed those of the copper alloys. In spite of the similarities in strength levels and defect microstructure, the stainless steels are able to sustain uniform strains >10%, at a reduced rate of strain hardening, prior to plastic instability, whereas in the copper alloys there is practically no uniform strain and plastic instability occurs immediately after yielding. The reasons for these differences in behavior are not understood at present. The formation of cleared dislocation channels in the defect microstructure has been observed in copper and copper alloys irradiated at temperatures ⩽ 200°C [19]. For stainless steels, the relationship between the loop microstructure and dislocation channeling at low strain rates and twinning at high strain rates has been discussed recently [20,21]. However, detailed TEM analysis of the size and frequency of dislocation channels in deformed irradiated stainless steel and copper alloys is needed before an understanding of the differences in deformation behavior can be developed.

In contrast to the stainless steels, both the tensile and fracture toughness properties of the copper alloys are
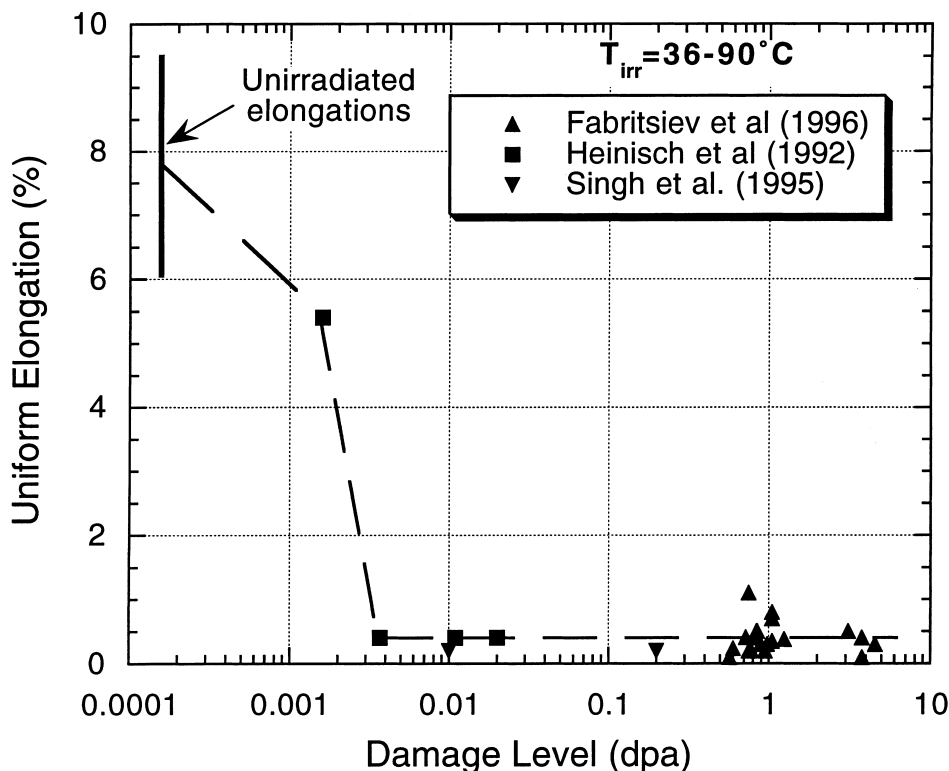
Fig. 7. The effect of low temperature neutron irradiation on the uniform elongation of several copper alloys; the rapid loss of E_u is a consequence of severe dislocation channeling.
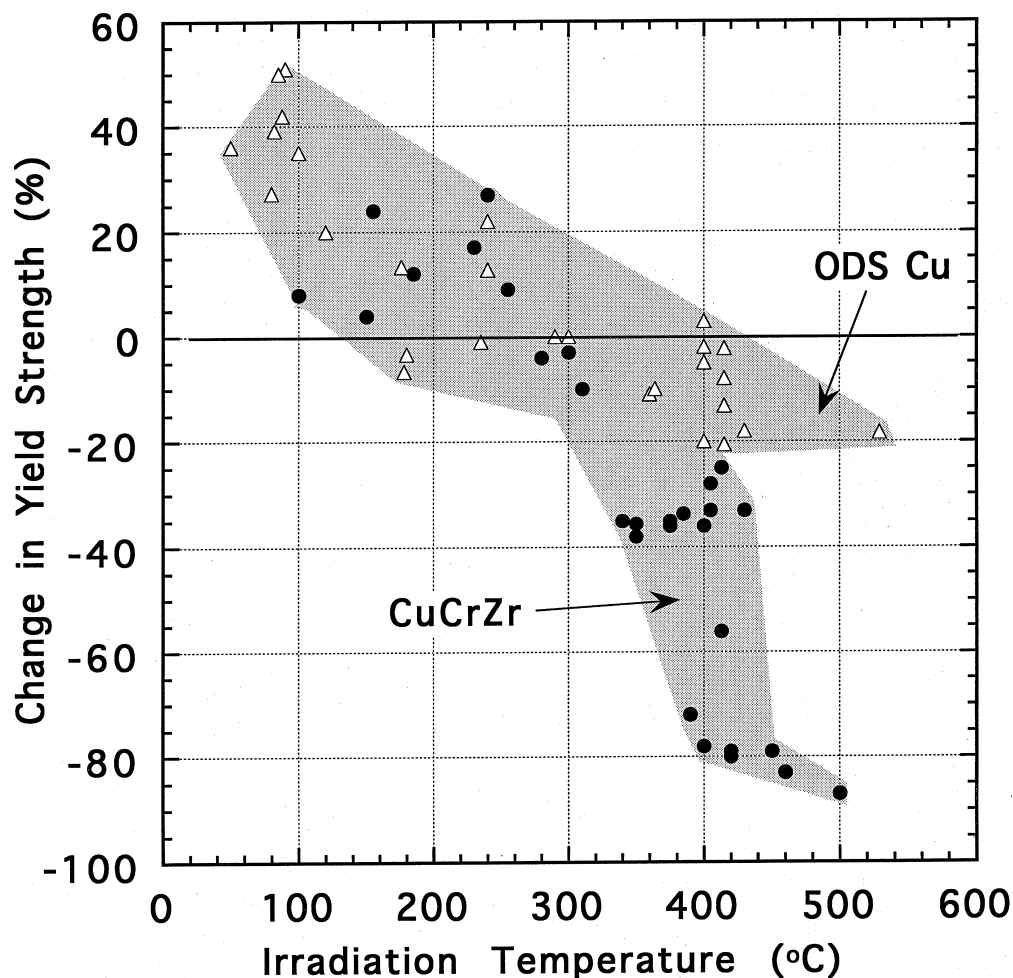
Fig. 8. Change in yield strength for copper alloys irradiated to ∼0.1 dpa. Rapid hardening and loss of uniform strain occurs for irradiation temperatures <250°C. A transition to radiation softening occurs at ∼275°C. A transition to radiation softening occurs at ∼275, with the GlidCop alloys being more resistant to softening than Cu–Cr–Zr [17].

relatively temperature sensitive over the operating temperature range of ITER components. This is particularly true for GlidCop Al25, which exhibits a fairly strong decline in YS, UE, and K_J over the range RT to 350°C. In addition, the tensile properties of GlidCop Al25 exhibit a significant strain rate sensitivity with increasing temperatures, and both YS and UE decrease with decreasing strain rates over the range 10^{-1}–10^{-4} s^{-1} [22]. The stronger temperature sensitivity of GlidCop Al25 is also reflected in the fracture toughness behavior, with K_J values dropping to <50 MPa $\sqrt{m}$ at 250°C. Unlike the stainless steels, there is a marked degree of anisotropy in the fracture properties of the copper alloys, with fracture resistance being particularly poor in the SL orientation in GlidCop Al25; that is with a crack in the plane of the plate and propagating in the extrusion direction [20].

The reduction in fracture resistance with increasing temperature is not observed when testing is carried out at dynamic strain rates (>1 s^{-1}). It has also been noted that the fracture toughness of GlidCop Al25 is improved by ∼50% when testing is carried out in vacuum rather than in air [23]. These two pieces of evidence suggest that oxygen chemisorption along grain boundaries could possibly be playing a role in lowering the fracture resistance of the ultra-fine grained GlidCop Al25. The presence of Zr in the Cu–Cr–Zr coupled with the lower strain rate sensitivity could be important factors in the superior fracture toughness behavior of the Cu–Cr–Zr alloy.

There are very few data on the effects of neutron irradiation on fracture toughness of the copper alloys. Alexander and Gieseke reported a severe reduction in fracture toughness at 250°C after irradiation of a
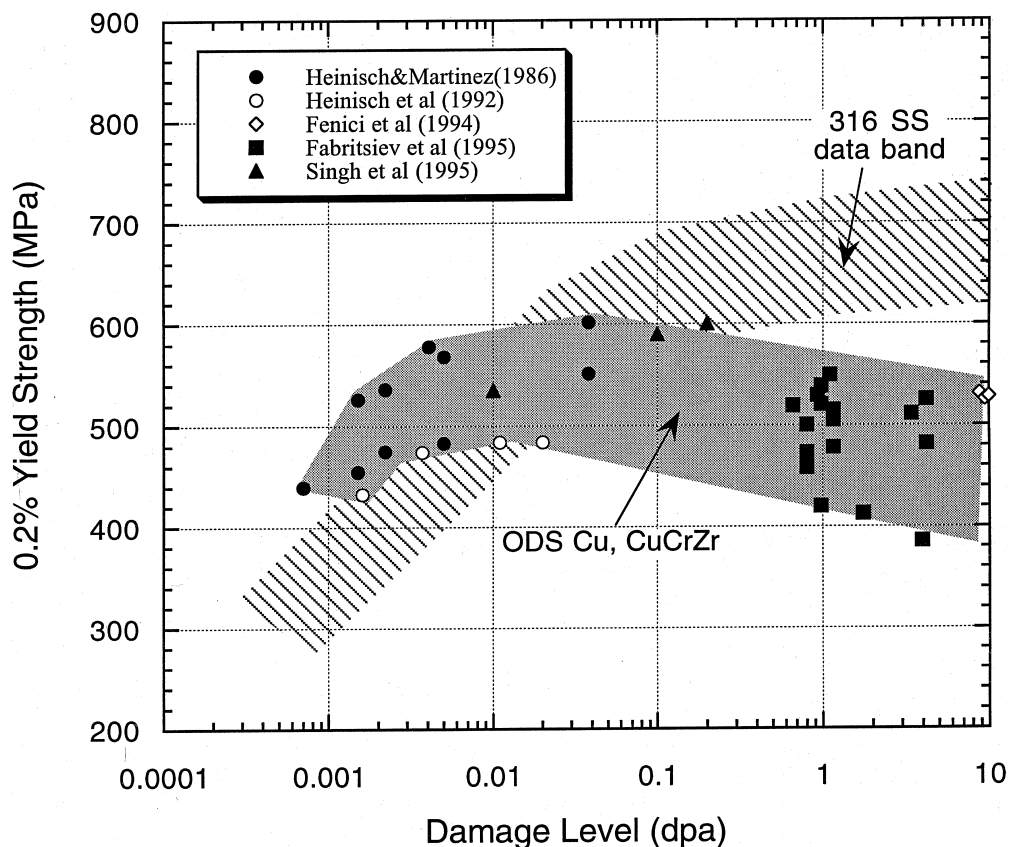
Fig. 9. Comparison of the fluence dependence of yield stress for 316 stainless steel and high strength copper alloys irradiated at temperatures in the range 60–200°C [17].

GlidCop Al15 alloy to only 0.3 dpa [24]. Data presented by Tähtinen et al. in these proceedings [25] show that irradiation to 0.3 dpa had relatively little effect on the fracture toughness of Cu–Cr–Zr at 50°C and 200°C, and resulted in a 50% reduction at 350°C. However, the initiation fracture toughness for GlidCop Al25 was reduced by a factor of 3 at all temperatures so that values of $J_{0.2BL}$ were reduced to 28 kJ/m^2 at 50°C and to <5 kJ/m^2 at 200°C and 350°C.

From the foregoing, it is evident that there are several problem areas regarding the effectiveness of high strength copper alloys as heat sink materials in the ITER environment, namely (a) the loss of strain hardening capacity and uniform elongation in both alloys at low doses for temperatures <200°C, (b) the onset of radiation-induced softening in Cu–Cr–Zr for irradiation at temperatures >300°C, (c) the reduction in fracture toughness and UE of GlidCop Al25 with increasing temperature and decreasing strain rate, (d) the poor fracture resistance of GlidCop Al25 in the SL direction, and (e) the radiation-induced reduction in fracture toughness of GlidCop Al25 following irradiation to 0.3 dpa at 50–300°C. To a certain extent, these deficiencies

in performance may be accommodated by making design changes to adjust operating temperature ranges and stress levels. It is also possible that the impact of radiation hardening and flow localization can be mitigated by periodic in situ annealing of components during the machine bake-out cycle. A significant amount of annealing of SFT occurs at temperatures ⩾ 300°C and reductions in yield strength [26] and increases in ductility [27] have been observed for annealing times of 1–50 h. It is not known if fracture toughness can be recovered, and the effects of repeated periods of irradiation and annealing on microstructure and deformation behavior remain to be explored.

4. Effects of thermal cycles in component fabrication

The ITER FW/shield is a complex structure. A 20 mm thick copper alloy heat sink is bonded on one side to the water cooled stainless steel shield and on the plasma side it is bonded to a 10 mm thick layer of plasma facing materials; Be is used at the primary wall and W is used for the lower baffle. The heat sink carries an array of

thin-walled stainless steel tubes for water cooling. The fabrication sequence required to assemble a module is correspondingly complex, with as many as 10 different operations involving 3–4 HIP bonding treatments at temperatures in the range 930–1050°C [28]. Because of the size of the modules, cooling rates from the bonding temperature are relatively slow, and the repeated heating and slow cooling cycles affect the final microstructure and microchemistry of the fabricated product. This is particularly true for the Cu–Cr–Zr alloy, which requires a high super-saturation of Cr in solution prior to the aging treatment at 475°C to ensure proper development of the optimal strength and thermal conductivity. Achievement of optimal properties requires a cooling rate from the solution treatment temperature of at least ~20°C/s [29]. For the cooling rates characteristic of the FW module fabrication (~0.1°C/s), there is insufficient Cr retained in solution for any significant age hardening to occur, and a post-HIPping aging treatment becomes superfluous. As a result of these slow cooling rate conditions, it is not possible to develop a room temperature YS greater than 70–80 MPa, compared to ~310 MPa for a fully heat treated alloy. In addition, thermal conductivity is lowered to ~69% IACS, compared to ~76% for the rapidly quenched and aged alloy [30]. The situation is somewhat better for some divertor components where production cooling rates of 2–4°C/s are achievable by gas cooling. In this situation, yield strength of ~220 MPa can be developed during aging [30].

This problem does not arise for the oxide-dispersion-strengthened GlidCop Al25 and both thermal and mechanical properties are relatively immune to repeated production cycles. For the 316LN-IG, although repeated heating to temperatures >1050°C is likely to induce some grain growth, there should be very little effect on mechanical behavior. However, it is possible that some changes in stress corrosion cracking behavior could occur due to changes in grain boundary microchemistry. Since the data bases on irradiation performance have been derived from materials subjected to a single conventional heat treatment, the impact of repeated production cycles on radiation response needs to be assessed. For the GlidCop Al25 and 316LN-IG, the effect of repeated thermal cycles are likely to be minimal. However, since the slow cooling rate has such a major effect on the microstructure of Cu–Cr–Zr, a fairly extensive study of irradiation performance in the as-fabricated condition will be needed to provide design data.

5. Properties of GlidCop Al25/316LN bi-layers

The primary approach selected for the FW structure is to use HIP to bond a GlidCop Al25 heat sink to the 316LN-IG shield. For the ITER divertor, a range of bonding methods is being evaluated to bond plasma-

facing materials (Be, W, CFCs) to a copper alloy heat sink (Cu–Cr–Zr, GlidCop Al25). Methods being evaluated include diffusion bonding, brazing, explosion bonding, plasma spray, and the use of various types of interlayers [31]. The mechanical behavior of thick section bi-layers is a relatively unexplored area of fusion materials science, and one of considerable importance to any fusion system where it is necessary to bond plasma-facing materials to a heat sink. In the case of the ITER FW, the primary and secondary loads are designed to be borne by the stainless steel structure, which retains a high level of toughness under irradiation. The main performance issue is whether or not the bi-layer (leaving aside the question of the plasma-facing Be layer) can withstand machine lifetime thermal–mechanical loading and disruption loads without losing its ability to transfer heat out of the system. The growth of cracks along the interface leading to extensive delamination is of prime concern in this regard.

A comprehensive assessment of the mechanical properties of small-scale panels of copper alloy/stainless steel bi-layers produced in the US was reported by Leedy [32]. He reported strong uniform bonds with good tensile and shear strength characteristics produced by HIP of 15 mm thick plates of GlidCop Al25 to 10 mm thick plates of 316LN-IG at 980°C. In fatigue tests carried out in 4-point bending and in fracture toughness testing, it was shown that the dominant failure mode was by rapid crack growth in the GlidCop parallel to and adjacent to the interface. Researchers in Japan [33] and in the EU [34] have similarly reported poor fracture resistance of GlidCop Al25 in this direction. The effect on neutron irradiation on the deformation and fracture behavior of copper alloy/stainless steel bi-layers is currently under investigation by the authors. A miniaturized 3-point bend bar, machined from the bi-layer such that the bond interface runs at 45° to the long axis of the specimen has been adopted which enables interrogation of the bond by cracks approaching at 45° from either the copper side or from the stainless steel side. With this geometry, it was found that stable fatigue cracks could be developed at room temperature in the 316LN-IG and in the Cu–Cr–Zr. However, in the GlidCop Al25, fatigue cracks propagated only a short distance before turning and running in a direction parallel to the interface. When a fatigue crack approached the interface from the stainless steel side, rapid crack propagation and delamination occurred in the GlidCop Al25 and in a direction parallel to and adjacent to the bond interface. Finite element modeling using ANSYS analysis of the miniature specimens loaded in 3-point bending indicated the development of large shear stresses along the interface, away from the center of the specimen and towards the thinner section of the copper wedge. In part, this arises from the mismatch in elastic constants between the copper and the stainless steel. As mentioned earlier,

　　　　A.F. Rowcliffe et al. / Journal of Nuclear Materials 258–263 (1998) 183–192

fracture toughness testing of GlidCop Al25 using disk compact specimens revealed a severe anisotropy with poor fracture resistance in the S–L direction, which is the direction oriented parallel to the bond interface during the HIP process. It appears, therefore, that the 316LN/GlidCop Al25 bi-layer material is prone to failure by a shear delamination along the weak microstructural direction in the GlidCop Al25.

This preliminary work raises serious doubts regarding the application of GlidCop Al25 as the heat sink material for the ITER FW. It also raises numerous issues regarding the methodology for assessing the fracture resistance of bi-layers and their load bearing capacity, not only in the FW but also for the plasma facing material/heat sink bi-layers being developed for the divertor. Additional finite element analysis is needed to investigate the relevance of the stress fields and constraint in the subsize specimens in determining failure modes and setting failure criteria in full-size components. The influence of radiation-induced changes in yield strength and deformation mode need to be investigated using a combination of finite element modeling and experimental methods.

Acknowledgements

References

[1] A.A. Tavassoli, Fusion Eng. Des. 29 (1995) 371–390.
[2] R.S. Solomon et al., J. Nucl. Mater. 233–237 (1996) 524.
[3] K. Ioki et al., these Proceedings.
[4] P.J. Maziasz, J. Nucl. Mater. 205 (1993) 118.
[5] S.J. Zinkle et al., J. Nucl. Mater. 206 (1993) 266.
[6] E.H. Lee et al., in: J.R. Holland, L.K. Mansur, D.I. Potter (Eds.), Proceedings of AIME Conference on Phase Stability During Irradiation, Pittsburgh, PA, 1980, p. 191.
[7] M. Horiki, M. Kiritani, J. Nucl. Mater. 212–215 (1994) 246.
[8] G.E. Lucas, J. Nucl. Mater. 206 (1993) 287.
[9] J.E. Pawel et al., J. Nucl. Mater. 239 (1996) 126.
[10] G.E. Lucas, Mat. Res. Soc. Symp. Proc., vol. 439, Materials Research Society, 1997, p. 425.
[11] S. Majumdar, Fusion Eng. Design 29 (1994) 158.
[12] D.J. Alexander et al., Proceedings of the 17th International Symposium on the Effects of Radiation on Materials, ASTM STP 1270 (1996) 945.
[13] E.V. van Osch et al., these Proceedings.
[14] G.E. Lucas, J. Nucl. Mater. 206 (1993) 287.
[15] S.J. Zinkle, Proceedings of the 15th International Symposium on the Effects of Radiation on Materials, ASTM STP 1125 (1992) 813.
[16] B.N. Singh, S.J. Zinkle, J. Nucl. Mater. 206 (1993) 212.
[17] S.A. Fabritsiev et al., J. Nucl. Mater. 233–237 (1996) 127.
[18] S.J. Zinkle et al., J. Nucl. Mater. 212–215 (1994) 132.
[19] J.V. Sharp, Radiat. Effects 14 (1972) 71.
[20] S.M. Bruemmer et al., Mat. Res. Soc. Symp. Proc., vol. 437, Materials Research Society, 1997, p. 437.
[21] S.G. Song et al., Acta Mater. 45 (2) (1977) 501.
[22] S.J. Zinkle, W.S. Eatherly, Effect of test temperature and strain rate on the tensile properties of high strength, high-conductivity copper alloys, Fusion Materials Semiannual Progress Report, DOE/ER-0313/21, December 1996, p. 165.
[23] D.J. Alexander, private communication.
[24] D.J. Alexander, B.G. Gieseke, Fracture toughness and fatigue crack growth of ODS copper, Fusion Materials Semiannual Progress Report, DOER/ER-0313/19, December 1995, p. 189.
[25] S. Tähtinen et al., Effects of neutron irradiation on fracture toughness behavior of copper alloys, these Proceedings.
[26] M.J. Makin, Radiation effects, in: W.F. Sheely (Ed.), Metallurgical Society Conference, vol. 37, Gordon & Breach, New York, 1967, p. 627.
[27] B.N. Singh, private communication.
[28] K. Mohri, work in progress at ITER Joint Central Team, Garching, Germany.
[29] T. Toda, Trans. Japan Inst. Met. 11 (1970) 24, 30.
[30] S.J. Zinkle, W.S. Eatherly, Effect of heat treatments on the tensile and electrical properties of high-strength, high-conductivity alloys, Fusion Materials Semiannual Progress Report, DOE/ER-0313/22, June 1997, p. 143.
[31] M.A. Ulrickson, presented at 8th Int. Conf. on Fusion Reactor Materials, Sendai, Japan, 1997.
[32] K. Leedy, PhD thesis, Department of Math. Science and Eng., University of Illinois at Urbana-Champaign, July 1997.
[33] T. Hatano et al., these Proceedings.
[34] G. LeMarois et al., Advanced joining techniques for ITER modules manufacturing, Note Technique DEM, No. 32/97, CEA/CEREM, Grenoble, May 1997.